Chapter 13
Monte Carlo Methods to Model Radiation Interactions and Induced Damage

Antonio Muñoz, Martina C. Fuss, M.A. Cortés-Giraldo, Sébastien Incerti, Vladimir Ivanchenko, Anton Ivanchenko, J.M. Quesada, Francesc Salvat, Christophe Champion, and Gustavo García

Abstract This review is devoted to the analysis of some Monte Carlo (MC) simulation programmes which have been developed to describe radiation interaction with biologically relevant materials. Current versions of the MC codes Geant4 (GEometry ANd Tracking 4), PENELOPE (PENetration and Energy Loss of Positrons and Electrons), EPOTRAN (Electron and POsitron TRANsport), and

AQ1

A. Muñoz (✉)
Centro de Investigaciones Energéticas, Medioambientales y Tecnológicas (CIEMAT),
28040 Madrid, Spain
e-mail: roldan@ciemat.es

M.C. Fuss • G. García
Instituto de Física Fundamental, Consejo Superior de Investigaciones Científicas,
28006 Madrid, Spain
e-mail: mc.fuss@iff.csic.es; g.garcia@iff.csic.es

M.A. Cortés-Giraldo • J.M. Quesada
Departamento de Física Atómica, Molecular y Nuclear, Universidad de Sevilla,
E-41080 Sevilla, Spain
e-mail: miancortes@us.es; quesada@us.es

S. Incerti
Université Bordeaux 1, CNRS/IN2P3, Centre d'Etudes Nucléaires de Bordeaux Gradignan,
CENBG, BP120, 33175 Gradignan, France
e-mail: incerti@cenbg.in2p3.fr

V. Ivanchenko
Laboratoire de Physique Moléculaire et des Collisions, Institut de Physique,
Université Paul Verlaine-Metz, 57078 Metz Cedex 3, France
e-mail: Vladimir.Ivantchenko@cern.ch

A. Ivanchenko
Université Bordeaux 1, CNRS/IN2P3, Centre d'Etudes Nucléaires de Bordeaux Gradignan,
CENBG, BP120, 33175 Gradignan, France

Geant4 Associates International Ltd, Manchester, United Kingdom
e-mail: Anton.Ivantchenko@cern.ch

G. García and M.C. Fuss (eds.), *Radiation Damage in Biomolecular Systems*, Biological and Medical Physics, Biomedical Engineering,
DOI 10.1007/978-94-007-2564-5_13,

LEPTS (Low-Energy Particle Track Simulation). Mean features of each model, as the type of radiation to consider, the energy range covered by primary and secondary particles, the type of interactions included in the simulation and the considered target geometries are discussed. Special emphasis lies on recent developments that, together with (still emerging) new databases that include adequate data for biologically relevant materials, bring us continuously closer to a realistic, physically meaningful description of radiation damage in biological tissues.

13.1 Introduction

Decades ago, the Monte Carlo (MC) method started to be used for the simulation of radiation transport [1–4]. It consists in the numerical determination of multiple particle trajectories, so-called particle "histories", across an absorber material. This is achieved by following each incident particle through the subsequent collisions it undergoes and applying specific rules each time one of the expected interaction processes occurs. This approach is particularly useful in complex conditions where deterministic calculations would be unfeasible. By sampling a sufficiently large number of tracks and averaging over the ensemble obtained, MC simulation can – at least in principle – predict radiation-matter interactions exactly.

While the precision (given by the statistical uncertainty) of a MC result depends on computational parameters, the accuracy achieved in practice depends on the existing knowledge of the elementary collisional processes involved and on their implementation in the interaction model. Since the first computer programmes became available to a wider public [5–8], succesive codes or versions have steadily evolved in order to include new insights regarding the underlying physics (e.g. through database updates or a more differentiated treatment of the given collision types). Also through improvements in practical aspects such as the definition of composition and geometry of the simulated absorbers, graphical output, etc., using MC codes in a steadily broader field of applications and by a wider community of users was facilitated. At the same time, there have been computational advances aimed mainly at reducing calculation time (thus increasing a code's "efficiency"), the most notable developments probably being the introduction of the "condensed history" technique [9] (an approximation for multiple scattering which is the base of many modern MC codes) and the application of variance-reduction

F. Salvat
Facultat de Física (ECM), Universitat de Barcelona, Societat Catalana de Física (IEC), 08028, Barcelona, Spain cesc@ecm.ub.es

C. Champion
Université Bordeaux 1, CNRS/IN2P3, Centre d'Etudes Nucléaires de Bordeaux Gradignan, CENBG, BP120, 33175 Gradignan, France

Laboratoire de Physique Moléculaire et des Collisions, Institut de Physique, Université Paul Verlaine-Metz, 57078 Metz Cedex 3, France champion@univ-metz.fr

techniques [10,11] which reduce statistical uncertainty. Concerning radiation effects in biomolecular systems, the adaptation of the interaction model for use at lower energies [12, 13, later 14, 15] and modifications in electron physics in order to distinguish different inelastic processes [16,17] have constituted important advances in MC modelling.

Today, a variety of MC codes are available for simulating radiation-matter interactions. Amongst the most important ones, there are Geant4 [18] which origins are at the European Organization for Nuclear Research (CERN) and is being developed and maintained by an international collaboration, EGS4 [19], developed at Stanford Linear Accelerator Centre and now maintained as the EGSnrc [20] version by the National Research Council of Canada, ITS [21], MCNP [22] from Los Alamos National Laboratory, PENELOPE [15], PARTRAC [23], EPOTRAN [24], and LEPTS (Low-Energy Particle Track Simulation, [16, 25]). Principal differences can be found in the interaction models utilized, the origin and nature of the input databases, and the kind of output data and representation. Their applications currently range from high-energy physics (e.g. detector responses and shielding requirements) over electron microscopy to medical physics.

There, rapid developments – especially in the last decade – have lead from initially general programmes used only for comparative studies to user-friendly, specialized codes that are clinically applicable to a growing range of situations. Additionally to treatment verification or planning systems, MC calculation is extending to uses including diagnostic imaging and linac beam simulation (Chap. 19). However, many efforts in the biomedical context still focus on modelling radiation transport and damage induced in patient tissue.

A complete (from the physics point of view) simulation tool for modelling radiation damage in biomaterials should be able to model all possible combinations of:

– different tissues such as muscle, bone, tumour, lung, etc.
– different radiation types (photons, electrons, heavy charged particles)
– different energies/spectra, including that of secondary particles
– incident radiation geometries

Ultimately, it would be interesting to include the effects of reactive molecular species produced and biological response factors. This would provide a detailed view of the molecular damage induced and the related bio-functional impact at different scales.

In the following sections, we describe the current versions of the MC codes Geant4 (GEometry ANd Tracking 4), PENELOPE (PENetration and Energy LOss of Positrons and Electrons), EPOTRAN (Electron and POsitron TRANsport), and LEPTS (Low-Energy Particle Track Simulation). Special emphasis lies on recent developments that, together with (still emerging) new databases that include adequate data for biologically relevant materials, bring us continuously closer to a realistic, physically meaningful description of radiation damage in biological tissues.

13.2 Extension of the Geant4 Monte Carlo simulation toolkit for the modeling of radiation biological damages

13.2.1 The Geant4 Monte Carlo simulation toolkit

The Geant4 Monte Carlo simulation toolkit offers a general-purpose platform for the simulation of particle-matter interactions [18, 26, 27]. It includes a significant set of components for geometry description, particle definition, navigation and tracking, electromagnetic fields, physics models for electromagnetic, hadronic, optical, photo-nuclear and electro-nuclear interactions, event scoring, visualization and management of software components. Improvements and extensions of Geant4 capabilities continue, while its physics models are refined and results are accumulated. Improvement of Geant4 simulation performance is provided thanks to validation efforts and physics comparisons against data in collaboration with different experiments and user groups. The toolkit is developed by an international collaboration of about a hundred physicists and software engineers and Geant4 users participate actively in the verification and in the validation of the software. The development of Geant4 follows the open-source strategy: the source software is entirely accessible and freely downloadable via the Geant4 web site (http://www.geant4.org).

The toolkit is capable of modeling a large variety of physical processes for electromagnetic, optical and hadronic interactions. Electromagnetic interactions of photons and charged particles with matter are available in two alternative sub-packages, the "standard" electromagnetic sub-package which covers interactions from 1 keV up to 10 PeV, and the "low energy" electromagnetic sub-package which is applicable down to ∼100 eV. These sub-packages include processes describing ionization, bremsstrahlung, electron-positron pair creation, Compton scattering, single and multiple Coulomb scattering, Rayleigh scattering, photoelectric effect, and other processes [27].

Geant4 hadronic physics sub-packages include a large variety of physics models, which are complementary or sometimes alternative to each other [27] including models of high energy inelastic interactions based on string theories and models for moderate energy cascades, pre-equilibrium, low energy precise neutron transport, nuclear deexcitation, elastic and quasi-elastic scattering. At run time, depending on projectile particle type and energy, corresponding electromagnetic and hadronic models are selected.

Originally the development of Geant4 physics models focused on the simulation of High Energy Physics experiments, such as the experiments at the Large Hadron Collider at the European Organization for Nuclear Research (CERN, Ge-neva, Switzerland). Thanks to the use of object-oriented technology (C++), the toolkit was designed to be universal, taking into account requirements from other application domains involving particle-matter interactions. With time, new physics models and other software relevant to various medical and space applications were added. These domains also include biomedical physics and space physics, from micrometer biological cells [28] up to planetary scales [29].

Geant4 is currently being extended for the modeling of biological damage from ionizing radiation in the framework of the "Geant4-DNA" project which was initiated in 2001 by the European Space Agency [30].

13.2.2 The Geant4-DNA project

The Geant4-DNA project proposes to extend Geant4 for radiobiological damage simulation at the DNA scale in the context of long duration exposition to cosmic radiation, for example during long stays aboard the International Space Station or for future manned exploration missions of the Solar System. Applications in medical physics, such as track structure simulations for high-LET proton and hadrontherapy, are also foreseen. This project is an activity of the Geant4 collabo-ration and its developments are part of the electromagnetic package of Geant4. Since the latest release of the Geant4 toolkit (release 9.4, December 2010) Geant4-DNA proposes to Geant4 users a set of physical models for microdosimetry de-scribing the interactions of electrons, protons, neutral hydrogen atoms, helium par-ticles of different charged states and a few heavier ions (C, N, O, Fe - preliminary) in liquid water, the main component of biological tissues. Physical interactions in-clude elastic scattering, electronic excitation, ionization and charge exchange. These models take into account a fine description of the water molecule, including its five electronic excitation levels, as well as the four valence and K shells for ionization. Vibrational excitation and dissociative attachment for electrons have also been included for the simulation of thermalization of sub-excitation electrons [31]. The lowest reachable energies are a few eVs for electrons, $\sim$100 eVs for protons and neutral hydrogen, $\sim$1 keV for Helium and a few MeV for heavier ions. These models have been recently compared to experimental cross sections in the vapor phase as well as to international recommendations [32]. For illustration, total cross sections for electrons in the [4 eV – 100 keV] range are shown in Fig. 13.1. The corresponding models are described in [31, 32].

Geant4-DNA models do not use any condensed history approximation and simulate explicitly step-by-step all interactions with water, a necessary require-ment for track structure simulations at the scale of the DNA molecule. Conse-quently, their usage requires significant CPU resources and is not recommended at high energies. However, since the 9.4 release of the Geant4 toolkit, these models can be combined with other electromagnetic physics models available in Geant4. It is for example possible to apply them in conjunction with "standard" electro-magnetic physics models which use condensed history techniques, are very CPU efficient especially at higher energies (>10 MeV), and are adapted to larger scales. Using this combination, Geant4-DNA models can be applied to selected geometrical regions of the simulated setup within a specified energy range. A dedicated so-called "advanced example" named "microdosimetry" is available in the Geant4 toolkit in order to explain to users how to perform this multi-scale combination of models.

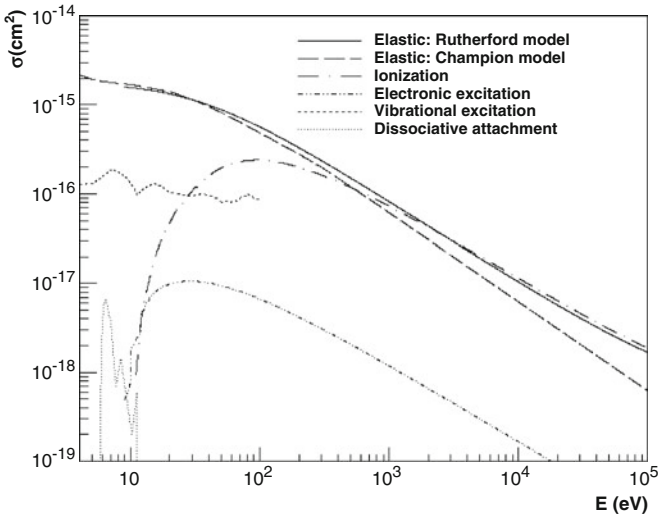

Fig. 13.1 Total cross section models for electrons in the [4 eV – 100 keV] range in liquid water available in the Geant4-DNA extension of the Geant4 toolkit (release 9.4, December 2010). The corresponding physical processes are: elastic scattering (two alternative models are available in Geant4-DNA, the screened Rutherford model – solid line – and the Champion's model – long-dashed curve –), ionization (dashed-dotted curve), electronic excitation (dashed-dotted-dotted curve), vibrational excitation (short-dashed curve) and dissociative attachment (dotted curve)

13.2.3 Modeling of biological damages

Geant4 combines simulations of direct effects of high energy radiation and low-energy secondary effects. High energy hadronic elastic and inelastic models sample interactions of primary particles with nucleons in the nucleus. After gener-ating high energy secondaries, the nucleus is left in an excited state, which should be de-excited to a thermalized state by a pre-equilibrium model. The final de-excitation is provided by de-excitation models. These low-energy final state mod-els are responsible for sampling the multiplicity of neutrons, protons, light ions and isotopes, which affects the overall picture of hadron transport and defines the major part of direct hadron/ion effects inside biological objects.

The modeling of direct biological damages due to excitation and ionization on biological targets such as DNA requires physics models down to very low ener-gies as described above. First estimations of direct DNA single-strand breaks and double-strand breaks yields obtained with the Geant4-DNA physics models have been recently published for MeV protons in liquid water [33] and show a general agreement with reference Monte Carlo and experimental data.

The modeling of ionizing radiation non-direct effects requires specific physico-chemical and chemical processes for the production, diffusion and mutual interac-tions of molecular species produced from water radiolysis. These molecular spe-cies are responsible for non-direct damages to the DNA molecule which become

dominant for low-LET particles such as electrons. Although Geant4 cannot handle mutual interactions between particles, Geant4-DNA is currently being extended for the simulation of such physico-chemistry processes.

These developments should become publicly available soon in upcoming releases of the general-purpose Geant4 simulation toolkit. We expect they will offer users an open-source alternative to already existing advanced codes [34] usually designed for specific applications and not easily accessible.

13.3 PENELOPE

PENELOPE is a general-purpose Monte Carlo code system for the simulation of coupled electron-photon transport in arbitrary materials, which has been developed at the University of Barcelona over the last 15 years [14, 35, 36]. The name, an acronym for "PENetration and Energy LOss of Positrons and Electrons", was inherited from earlier works of the authors on the transport of low-energy electrons in solids, where the conventional detailed simulation (i.e., interaction by interaction) is applicable. This background naturally lead to the adoption of mixed simulation schemes (class II schemes in the terminology of Berger [9]) for electrons and positrons, which is the most characteristic feature of PENELOPE.

PENELOPE allows the simulation of electron-photon showers in material systems consisting of homogeneous bodies with arbitrary chemical compositions, for an energy range from 50 eV to 1 GeV (although the interaction database extends down to 50 eV, results for energies less than about 1 keV should be regarded as semi-quantitative). The interaction models implemented in the code are based on the most reliable information currently available, limited only by the required generality of the code. These models combine results from first-principles calculations, semi-empirical models and evaluated databases.

The core of the code system is a Fortran subroutine package that generates electron-photon showers in homogeneous materials. These subroutines are invoked from a main steering program, to be provided by the user, which controls the evolution of the tracks and keeps score of the relevant quantities. The code system also includes a flexible subroutine package for automatic tracking of particles within quadric geometries (i.e. systems consisting of homogeneous bodies limited by quadric surfaces) and a geometry viewer and debugger. A generic main program, called PENMAIN, allows the simulation of a variety of radiation sources in arbitrary quadric geometries; the user can define impact detectors and energy-deposition detectors to extract information from the simulation. The operation of PENMAIN is completely controlled from an input file. The latest public version of PENELOPE, released in 2008, is available from the OECD Nuclear Energy Agency Data Bank (http://www.nea.fr).

PENELOPE has been applied to a wide variety of problems in dosimetry, microdosimetry, radiotherapy, radiation protection, nuclear spectroscopy, electron microscopy, electron probe microanalysis, etc. A comprehensive comparison of

simulation results with experimental data available from the literature [37] for electrons with initial energies ranging from a few keV up to 1 GeV demonstrated the reliability of the adopted interaction models and tracking algorithm.

13.3.1 Interaction models

Interactions with the material change the energy and direction of movement of the transported particle, and may also produce secondary particles. PENELOPE combines numerical and analytical total and differential cross sections (DCS) for the different interaction mechanisms. These cross sections are necessarily approximate. For example, the cross sections for photoelectric absorption pertain to free atoms and, therefore, possible extended x-ray absorption fine structure effects are disregarded. Similarly, the x-ray energies and the transition probabilities of excited atoms with inner-shell vacancies are those of free atoms and, consequently, the effect of aggregation on these quantities is neglected. Nevertheless, the structure of the code is flexible enough to allow the use of alternative, more elaborate physical models when needed. Details on the physics models can be found in the code manual [36] and in the review article by Salvat and Fernández-Varea [38].

The interaction mechanisms considered in PENELOPE, and the corresponding DCSs, are the following:

- Elastic scattering of electrons and positrons: numerical DCSs obtained from Dirac partial-wave analysis for the electrostatic potential derived from Dirac-Fock atomic electron densities, with the exchange potential of Furness and McCarthy for electrons. These cross sections were calculated using the program ELSEPA [39, 40].
- Inelastic collisions of electrons and positrons: Born DCS obtained from the Sternheimer-Liljequist generalised oscillator strength model [41, 42], with the density-effect correction. The excitation spectrum is modelled by a discrete set of delta oscillators, whose resonance energies are scaled so as to reproduce the mean excitation energies recommended in the ICRU Report 37 [43]. Thus, collision stopping powers calculated from this model agree closely with the tabulations in [43]. Optionally, the DCS can be renormalised to reproduce the collision stopping power read from an input file.
- Electron impact ionisation: numerical total cross sections for ionisation of K, L and M electron shells of neutral atoms, calculated by means of the distorted-wave (first) Born approximation with the Dirac-Hartree-Fock-Slater self-consistent potential [44].
- Bremsstrahlung emission by electrons and positrons: the energy of the emitted photons is sampled from numerical energy-loss spectra derived from the scaled cross-section tables of Seltzer and Berger [45, 46], optionally renormalised to reproduce the radiative stopping power read from the input file. The intrinsic angular distribution of emitted photons is described by an analytical expression –

an admixture of two "boosted" dipole distributions – [47] with parameters determined by fitting the benchmark partial-wave shape functions of Kissel, Quarles and Pratt [48].
- Positron annihilation: Heitler DCS for two-photon annihilation in flight.
- Coherent (Rayleigh) scattering of photons: Born DCS with atomic form factors and angle-independent effective anomalous scattering factors taken from the LLNL Evaluated Photon Data Library [49].
- Incoherent (Compton) scattering of photons: DCS calculated using the relativistic impulse approximation with analytical one-electron Compton profiles [50].
- Photoelectric absorption of photons: total atomic cross sections and partial cross sections for the K-shell and L- and M- subshells from the LLNL Evaluated Photon Data Library [49]. The initial direction of photoelectrons is sampled from Sauter's [51] K-shell hydrogenic DCS.
- Electron-positron pair production: total cross sections obtained from the XCOM program of Berger and Hubbell [52]. The initial kinetic energies of the produced particles are sampled from the Bethe-Heitler DCS, with exponential screening and Coulomb correction, empirically modified to improve its reliability for energies near the pair-production threshold.

Most of these interaction models pertain to free atoms. Usually, they are extended to compounds and mixtures by assuming the additivity approximation, that is, molecular cross sections are obtained by adding the cross sections of the atoms in a molecule. An exception occurs for inelastic collisions of electrons and positrons, where molecular binding effects can be accounted for appropriately by using the mean excitation energy of the compound material.

The current version of the code allows the simulation of polarized photon beams, with the state of polarization described by the Stokes parameters. However, secondary photons (i.e., characteristic x-rays and Auger electrons, as well as bremsstrahlung photons emitted by electrons or positrons) are assumed to be unpolarized.

13.3.2 Simulation algorithm and geometry routines

Particle histories are simulated from the initial energy down to the absorption energies selected by the user, at which particles are considered to be effectively absorbed in the medium. Secondary electrons and photons emitted with initial energy larger than the corresponding absorption energy are simulated after completion of each primary track. Secondary particles are produced in direct interactions (hard inelastic collisions, hard bremsstrahlung emission, positron annihilation, Compton scattering, photoelectric absorption and pair production) and as radiation (characteristic x rays and Auger electrons) following inner-shell ionisation. PENELOPE simulates the emission of characteristic x-rays and Auger electrons that result from vacancies produced in K-shells and L- and M-subshells by photoelectric absorption and Compton scattering of photons and by electron or positron impact. The relaxation

of these vacancies is followed until all vacancies have migrated to N and outer shells. The adopted transition probabilities were extracted from the LLNL Evaluated Atomic Data Library [53].

The simulation of photon tracks follows the usual detailed procedure, i.e., all the interaction events in a photon history are simulated in chronological order. Detailed simulation of high-energy electrons and positrons is impractical, because these particles undergo a large number of interactions in the course of their slowing down. Electron and positron trajectories are generated by means of a mixed (class II) algorithm [54] that allows the generation of electron tracks with a relatively small number of computational steps. Hard interactions, with scattering angle or energy loss larger than certain cutoff values, are simulated in a detailed way, i.e., by random sampling from the corresponding restricted DCS. The path length to the next hard interaction is sampled according to the energy-dependent mean free path for hard interactions. The combined effect of all soft interactions that occur along the trajectory segment between two consecutive hard interactions is simulated as a single "artificial" soft event (a random hinge) where the particle loses energy and changes its direction of motion. The energy loss and angular deflection at the hinge are generated according to a multiple-scattering approach that yields energy-loss distributions and angular distributions with the correct mean and variance.

The manual contains a detailed description of the sampling algorithms adopted to simulate the different interactions. Continuous distributions are sampled by means of the adaptive algorithm RITA (Rational Inverse Interpolation with Aliasing); Walker's [55] aliasing method is adopted to sample discrete distributions with large numbers of possible outcomes. These sampling methods are both robust and fast.

The subroutine package PENGEOM tracks particles in material systems consisting of homogeneous bodies limited by quadric surfaces. These subroutines have been tailored to minimize the numerical work required to locate the particle (i.e., to find the body where it is moving) and to determine intersections of the particle trajectory with limiting surfaces. PENGEOM can describe very complicated systems with up to 5,000 bodies and 10,000 limiting surfaces. Material bodies can be grouped in modules, which in turn are organized in a genealogical tree structure. When the tree of modules is properly defined, the speed of the geometry operations is largely independent of the complexity of the whole material system.

13.4 EPOTRAN: a full-differential Monte Carlo code for electron and positron transport in liquid and gaseous water

EPOTRAN (an acronym for Electron and POsitron TRANsport in water) is a home-made full-differential Monte Carlo (MC) simulation developed by Champion [24] for modelling electron and positron histories in liquid and gaseous water for impact energies ranging from 10 eV to 100 keV. All the induced collisional processes are studied in detail via theoretical differential and total cross sections calculated

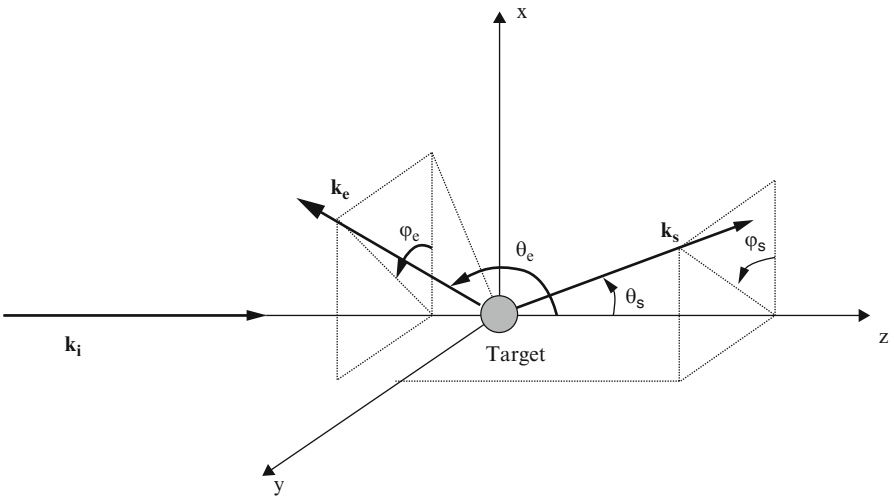

Fig. 13.2 Reference frame of the ionizing collision of a water target. $\boldsymbol{k}_i$, $\boldsymbol{k}_s$, and $\boldsymbol{k}_e$ represent the wave vectors of the incident, scattered and ejected electrons, respectively. The corresponding polar and azimuthal angles are denoted θ_s, φ_s and θ_e, φ_e, respectively

within the quantum mechanical framework by using partial wave methods. Water molecules are treated as point-like targets and therefore any potential energy associated with ionization, excitation or Positronium formation event is assumed to be locally deposited.

Under these conditions, EPOTRAN represents an event-by-event charged particle transport simulation which consists in a series of random samplings determining successively *i)* the distance travelled by the charged particle between two collisions, *ii)* the type of interaction that occurred and finally *iii)* the complete kinematics of the resultant particles (the primary - scattered - projectile as well as the potentially created secondary electron often called δ-ray).

Thus, if the selected interaction is an elastic scattering, the corresponding singly differential cross sections are sampled in order to determine the scattering direction, while the electron incident energy E_{inc} remains quasi unchanged, the energy transfer induced during elastic process being very small (of the order of meV). In the case of ionization, the kinetic energy of the ejected electron E_e is first determined by random sampling among the singly differential cross sections $d\sigma/dE_e$, while the ejection and scattering directions are respectively determined from the triply and doubly differential cross sections hereafter denoted $d^3\sigma/d\Omega_s d\Omega_e dE_e$ and $d^2\sigma/d\Omega_s dE_e$, where Ω_s refers to the scattering direction, Ω_e to the ejection direction and E_e to the energy transfer (see Fig. 13.2). The incident particle energy is finally reduced by $E_e + IP_j$, where the latter term corresponds to the ionization potential of the jth molecular subshell (with j ranging from 1 to 5 for the five water molecule subshells referred as $1b_1$, $3a_1$, $1b_2$, $2a_1$ and $1a_1$, respectively). As mentioned above, let us note that IP_j is considered as locally deposited, except if the selected interaction is inner-shell ($1a_1$) ionization. In this

case, Auger electrons with a kinetic energy $E_{Auger} = 467.6\,\text{eV}$ are produced and isotropically emitted, the remaining energy ($IP_5 - E_{Auger}$) being considered as locally deposited. If an excitation is selected, the relative magnitudes of all the partial excitation cross sections are randomly sampled for selecting an excitation channel n whose corresponding energy E_n is considered as locally deposited. The incident particle energy is then reduced by E_n whereas no angular deflection is assumed as experimentally observed. Finally, for positron energy $E_{inc} \geq IP_1 - I_{Ps}$ (where I_{Ps} corresponds to the Positronium binding energy), Positronium (Ps) formation may be considered. To do that, we first determine the target molecular subshell concerned by the capture process as well as the final Positronium state ($Ps(1s)$ or $Ps(2s)$) according to the relative magnitude of all the partial capture cross sections. The quantity ($IP_j - I_{Ps}$) is then assumed as locally deposited whereas the kinetic Positron energy E_{Ps} is simply determined from kinematical considerations ($E_{inc} + I_{Ps} = E_{Ps} + IP_j$). Finally, for computing velocity reasons we here assume that Positronium formation induces no angular deflection and then suppose that Positronium is ejected in a direction collinear to that of the incident positron. However, in a more sophisticated version of the code, Positronium ejection direction could easily be selected from the pre-calculated singly differential cross sections.

All these steps are repeated for all primary and secondary particles until their kinetic energy falls below a predetermined cut-off value, here fixed at $E_{th} = 7.4\,\text{eV}$, which corresponds to the electronic excitation threshold. Sub-threshold (sub-excitation) electrons and positrons are then assumed to deposit their energy where they are created. In fact, these low-energy species essentially induce vibrational and/or rotational excitations as well as elastic collisions whose total cross section becomes very large (about $20 \cdot 10^{-16}\,\text{cm}^2$), leading to a mean free path less than 1 nm. Therefore, assuming that these 'killed' particles stay where they have been created, introduces uncertainties smaller or of the order of 1 nm in the final energetic cartography.

Finally, note that multiple electronic processes are not taken into account in the current version of our code but should be implemented in the near future [56]. Similarly, we have neglected the contribution of Bremsstrahlung in the electronic and positronic slowing-down due to its minor influence in the energy range here considered ($E_{inc} < 1\,\text{MeV}$).

To describe the following-up of electrons and positrons in water, it is essential to address a large set of differential and total cross sections corresponding to the different types of interactions induced by the charged particles in the medium. In the following, we describe all these cross sections, whose calculation has been performed within the quantum-mechanic framework by using the partial wave expansion method.

13.4.1 The elastic scattering description

The perturbation potential induced by charged particles in water can be approximated by a spherically symmetric potential $V(r)$ composed of three distinct terms:

a static contribution $V_{st}(r)$ and two fine correction terms corresponding to the correlation-polarization and the exchange interactions, denoted $V_{cp}(r)$ and $V_{ex}(r)$, respectively. The total interaction potential can then be written as

$$\begin{cases} V(r) = V_{st}(r) + V_{cp}(r) + V_{ex}(r) & \text{for electrons,} \\ V(r) = -V_{st}(r) + V_{cp}(r) & \text{for positrons.} \end{cases}$$

In water vapour, the static potential was numerically calculated within the spherical average approximation from the target molecular wave functions. These latter have been taken from Moccia [57] who described the water molecule by means of single-centre wave functions, each of them being expressed in terms of Slater-type-orbital functions, all centered at a common origin (the oxygen atom). For liquid water, the situation being less trivial essentially due to the scarcity of available molecular wave functions (except those provided by theoretical calculations performed in the Dynamic Molecular framework), we have privileged an empirical approach, which consists in extrapolating the static potential from the experimental liquid water electron density recently reported by Neuefeind et al. [58] (see [59] for more details).

To treat the correlation and polarization effects, we have followed the recommendations of [60] who successfully introduced a correlation–polarization potential into the treatment of electron scattering by noble gas and mercury. Whereas the polarization contribution was treated by means of a polarization potential of the Buckingham type [61] for both electrons and positrons, correlation effects were introduced via different potentials, namely, that described by Padial and Norcross [62] for electrons and that reported by Jain [63] for positrons. Finally, the exchange process (only used for electrons) was treated via the phenomenological potential given by Riley and Truhlar [64]. Singly differential cross sections $d\sigma/d\Omega_s$ were then evaluated within the partial wave framework for both electrons and positrons in gaseous and liquid water whereas total cross sections were simply obtained by means of numerical integration (see Fig. 13.3).

13.4.2 The ionization treatment

In the 1st Born approximation, triply differential cross sections for both electrons and positrons are defined as

$$\begin{aligned} \sigma^{(3)}(\Omega_s, \Omega_e, E_e) &\equiv \frac{d^3\sigma}{d\Omega_s d\Omega_e dE_e} = \sum_{j=1}^{N_{MO}=5} \frac{d^3\sigma_j}{d\Omega_s d\Omega_e dE_e} \\ &= \sum_{j=1}^{N_{MO}=5} (2\pi)^4 \frac{k_1 k_s}{k_i} \left|[T_{ab}]_j\right|^2, \end{aligned} \tag{13.1}$$

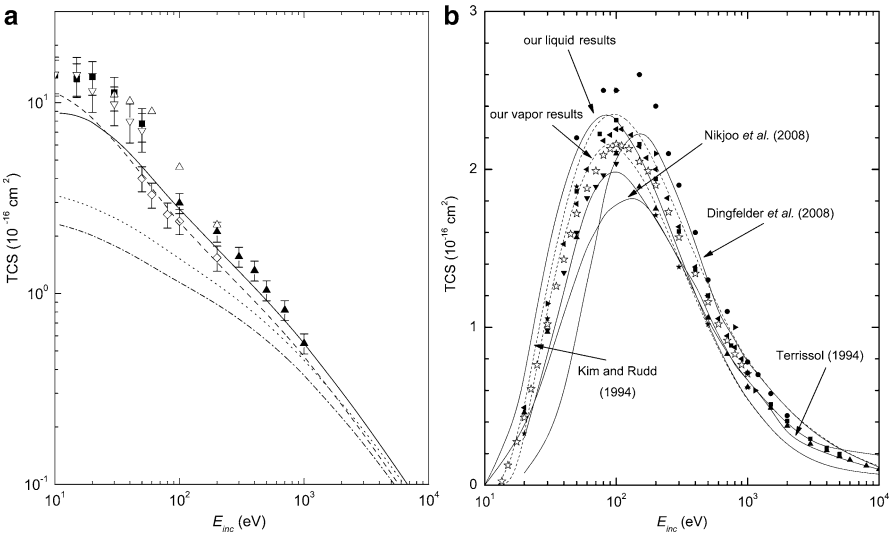

Fig. 13.3 Panel **(a)** Total cross sections (TCS) for elastic scattering of electrons in gaseous water (solid line) and liquid water (dashed line) compared to their equivalents for positrons (dotted and dash–dotted line, respectively). Experimental measurements taken from different sources are also reported for comparison (see [59] for more details). Panel **(b)** Total ionization cross sections versus the incident energy for both phases. Experimental measurements are also reported for comparison (see [56] for more details)

where the transition amplitude between the initial state labeled a and the final state labeled b, denoted $[T_{ab}]_j$, is expressed by

$$[T_{ab}]_j = \left\langle \Psi_b^j(\boldsymbol{r_0}, \boldsymbol{r_1}) \middle| V(\boldsymbol{r_0}, \boldsymbol{r_1}) \middle| \Psi_a^j(\boldsymbol{r_0}, \boldsymbol{r_1}) \right\rangle, \tag{13.2}$$

where $V(\boldsymbol{r}_0, \boldsymbol{r}_1)$ represents the interaction potential between the incident electron/positron and the target, which can be reduced as

$$V(\boldsymbol{r_0}, \boldsymbol{r_1}) = \frac{1}{|\boldsymbol{r_0} - \boldsymbol{r}_1|} - \frac{1}{r_0}. \tag{13.3}$$

Then, by using the well-known partial-wave expansion of the plane wave as well as that of the Coulomb wave, (13.1) may be written in a convenient analytical form from which doubly differential cross sections were obtained by analytical integration over the ejected electron direction whereas singly differential and then total cross sections were finally determined via numerical integrations (for more details, we refer the reader to our previous works [65, 66]).

Furthermore, contrary to the previous case where electronic density was simply needed for describing the elastic process, ionization treatment requires the knowledge of accurate target wave functions, what remains a difficult task essentially

due to the multi-centered nature of the water target. In this context, we have recently proposed a unified methodology to express the water molecular wave functions in both phases by means of a single-centre partial-wave description (see [56, 67] for more details). In brief, the wave functions have been carried out by using the Gaussian 03 program and computed at the Hartree-Fock level of theory by using the augmented, correlation-consistent, polarized-valence quadruple-zeta basis set (aug-cc-pvQZ) of Kendall *et al.* [68]. Geometry optimization has been done by including electronic correlation energy at the second-order Møller-Plesset perturbation theory (MP2, [69]). For the computations in the liquid phase we have used the polarizable continuum model (PCM) developed by Tomasi et al. [70] based on the representation of the liquid by a polarizable dielectric continuum having the static dielectric constant of water ($\varepsilon = 78.39$). Thus, a cavity was created in this continuum and a water molecule was placed in it. The molecule was then described quantum mechanically with a Hamiltonian including the electrostatic interactions with the surrounding dielectric medium. Once polarized by the molecular charges, the continuum creates a reaction potential inside the cavity, which in turn polarizes the molecule. The wave function was also obtained by an iterative computation using the so-called self-consistent reaction field approach.

The obtained wave functions were then here used as input data in our theoretical treatment developed for describing the water ionization induced by electron and positron impact in the energy range 10 eV–100 keV (see Fig. 13.3).

13.4.3 The excitation processes

Excitation includes all the processes that modify the internal state of the impacted target molecule (without secondary electron creation), each of them giving a non negligible contribution to the final energetic cartography. They include in particular: *i)* electronic transitions towards Rydberg states or degenerate states ($\tilde{A}_1B_1$, $\tilde{B}_1A_1$, diffuse band), *ii)* dissociative attachment leading to the formation of negative ions, *iii)* dissociative excitation, leading to excited radicals (H^*, O^* et OH^*), and in a minor part *iv)* vibrational and rotational excitations.

In order to account all the processes listed *i), ii)* and *iv)*, we have used the semi-empirical approach of Olivero et al. [71], whereas the dissociative excitation processes were treated via the approach proposed by Green and Dutta [72]. Moreover, following some experimental observations [73], we assume that excitation induces no angular deflection.

Finally, note that we have here assumed that electron- and positron-induced excitation could be treated in the same way considering recent experimental data on Neon which only reported slight differences in terms of total excitation cross sections between the two projectile types (see [74] for more details).

13.4.4 The Positronium formation

Due to its positive charge, the positron has the possibility to capture one of the target electrons leading in the final channel of the reaction to the formation of a bound system - consisting of an electron and a positron - called Positronium (*Ps*). A continuum distorted-wave final-state approximation was then developed for describing this process [75] in which the final state of the collision was distorted by two Coulomb wave functions associated with the interaction of both the positron and the active electron (the captured one) with the residual ionic target. Thus, singly differential and total cross sections were successively calculated within the well-known frozen-core approximation.

13.5 Low-Energy Particle Track Simulation

Following the discovery of radiation damage in biomolecular systems by low energy, sub-ionising electrons (see Chap. 1), the concept of nanodosimetry (a procedure to quantify radiation damage in nanovolumes) has developed. It aims at a detailed description of the interaction processes occurring in a nano-size target and their implications in terms of radiation damage (number of dissociative events, type of radicals generated, etc. . .). A molecular-level model suitable to obtain this kind of information requires a reliable and complete set of cross section data, not only as far as integral values are concerned, but also including differential data for all scattering angles. Since elastic processes are relevant to shape the particle track (and thus determine to which extent a particular nano-volume is irradiated), the desired level of detail cannot be achieved by using only high-energy approximations.

This section describes a new low energy particle track simulation (LEPTS) code, especially designed to provide interaction details at the nano-scale. The simulation procedure is based on an event-by-event Monte Carlo code which uses previously obtained experimental and theoretical electron and positron scattering cross sections and energy loss distribution functions as input parameters.

13.5.1 Interaction processes and input data

The main aspects to evaluate the reliability of a Monte Carlo model to achieve the above mentioned objectives, are the interaction processes considered and the probability distribution functions used to describe these processes. Our model is focused on electrons and positrons and, as far as their energies are concerned, we distinguish two different regions: above and below 10 keV. It has been shown [76] that for different molecules combining the atomic species H, C, N and O, the Born-Bethe approximation applies only for energies above 10 keV. This is due to the overestimation of the elastic cross section, which is even observed at an energy

of 5 keV. As such fast electrons can only distinguish the constituent atoms, a similar behaviour can be expected for most biomolecular systems at those energies. We will therefore use, for energies above 10 keV, the Born-Bethe theory [77] with an independent atom model representation [78] to describe the elastic and inelastic processes, as well as the energy deposition, in terms of the corresponding Bethe surfaces.

Below 10 keV, an appropriate description of the various processes and energy loss in terms of the scattering cross sections is required:

- The total scattering cross section provides the mean free path for the simulations.
- Differential and integral elastic cross sections are crucial to define the paths of the particles all along the energy degradation process down to their final thermalisation.
- Differential and integral inelastic cross sections for ionisation (total and partial), electronic excitation, rotational excitation, vibrational excitation, neutral dissociation and electron attachment. In the case of positrons, positronium formation is also considered and is critically important. Differential data is obtained as described in [17].

To illustrate the different approaches used to get a complete input data set, in the following sections we will only account for the case of molecular water.

13.5.1.1 Electron scattering experimental data

Total cross sections and energy loss spectra in the forward direction are derived in a transmission beam experiment [25]. Conventional electron energy loss experimental arrangements at Flinders and Liège Universities have been used to obtain high resolution (50–100 meV) electron energy loss spectra as a function of energy and scattering angle. By integrating the differential inelastic data, electron impact excitation cross sections for a given excitation energy are derived [79]. By combining electron-ion current measurements with time of flight spectrometry of the induced fragments [80], total and partial ionisation cross sections are measured from threshold up to 10 keV.

13.5.1.2 Positron scattering experimental data

Positron data are mainly provided by the Centre for Antimatter-Matter Studies positron beam line facility at the Australian National University. Simultaneous differential and integral cross section data are measured in a transmission beam experiment carried out under intense axial magnetic beam conditions. The design and operation principles of this experiment have been described in detail previously [81]. Additional positronium formation cross section data are also derived from the analysis of the transmission curves.

13.5.1.3 Electron scattering calculations

Differential and integral elastic, as well as integral inelastic, cross sections are calculated with an optical potential method, which is based on an independent atom representation followed by a screening-corrected addition rule procedure to account for molecular targets (IAM-SCAR). The first subjects of these calculations are the constituting atoms. We represent each atomic target by an optical potential, whose real part accounts for the elastic scattering of the incident electrons while the imaginary part represents the inelastic processes which are considered as 'absorption' from the incident beam. To construct this complex potential for each atom the real part of the potential is represented by the sum of three terms: (i) a static term derived from a Hartree-Fock calculation of the atomic charge distribution, (ii) an exchange term to account for the indistinguishability of the incident and target electrons and (iii) a polarisation term for the long-range interactions which depend upon the target dipole polarisability. The imaginary part then treats inelastic scattering as electron collisions. Later improvements [82] finally led to a model which provides a good approximation for electron-atom scattering over a broad energy range.

To calculate the cross sections for electron scattering from molecules, we follow the independent atom model (IAM) by applying what is commonly known as the additivity rule (AR). In this paradigm the molecular scattering amplitude is derived from the sum of all the relevant atomic amplitudes, including the phase coefficients. Alternatively, ICSs can also be derived from the relevant atomic ICSs in conjunction with the optical theorem [78]. An inherent contradiction between the ICSs derived from these two approaches was solved by employing a normalisation procedure during the computation of the DCSs [83]. A limitation of the AR is that no molecular structure is considered, so that it is typically only applicable above $\sim$100 eV. To reduce this limitation we introduced the SCAR method [84], which considers the geometry of a relevant molecule (atomic positions and bond lengths) by employing some screening coefficients. With this correction the range of validity might be extended to incident electron energies as low as $\sim$50 eV. Furthermore, for polar molecules such as water, additional dipole-excitation cross sections can be calculated to further extend the energy range of validity (to $\sim$10 eV). In the present implementation, rotational excitation cross sections for a free electric dipole are calculated by assuming that the energy transferred is low enough, in comparison to the incident energy, to validate the first Born approximation. Under these circumstances, we have calculated approximate rotational excitation cross sections for water at 300 K by weighting the population for the J-th rotational quantum number at that temperature and estimating the average excitation energy from the corresponding rotational constants.

13.5.1.4 Positron scattering calculations

A similar procedure has been followed to calculate positron scattering cross sections. In this case the atomic optical potential used for electrons has been replaced

by that proposed by Reid and Wadehra [85]. The other major differences for positron scattering compared to electron scattering, are that the positron scattering potential does not include an exchange term and the positronium formation channel is indirectly introduced by fixing the threshold energy for the absorption potential just at the positronium binding energy, i.e. 6.2 eV.

13.5.2 Monte Carlo simulation procedure

The basis of the Monte Carlo code used in our simulations has been published elsewhere [16]. It is an event-by-event simulation procedure, programmed in C++, which is compatible with other general purpose Monte Carlo codes like GEANT4 [18]. Other related tools, such as the Geant4-based Architecture for Medicine-Oriented Simulations (available from http://fismed.ciemat.es/GAMOS/), have been used to define the target geometries. Photon and high energy electron (above 10 keV) tracks are then simulated with that general code whereas low energy electrons (below 10 keV) and positrons are treated by LEPTS.

For an incoming low energy electron or positron, the free path in the medium is first sampled. Once the location of an event is defined, partial cross sections determine whether an elastic or inelastic process is to take place and call the appropriate interaction routine. For elastic collisions, the programme samples the outgoing particle's angle according to the distribution established by the corresponding differential cross sections. In the case of inelastic collisions, different sub-processes (with their relative frequency given by the corresponding partial cross sections value) handle the different types of interactions that are accessible depending on the particles' energy. First, the energy lost in the collision is determined as a fixed value (in the case of vibrational excitation) or from the electron energy loss distributions (for all other inelastic channels). Subsequently, the particles outgoing direction is sampled using the differential cross section expressed as a function of the momentum transfer (rather than the angle). If ionisation has taken place, a secondary electron is automatically generated and enters the simulation process with an energy given by the energy lost by the primary electron less the ionisation energy and moving in the direction obtained when applying linear momentum conservation. Secondary electron or positron tracks are then fully simulated with the same procedure.

13.5.3 Some results

As an example of the results that can be obtained with our LEPTS procedure, 50 single tracks corresponding to 15 keV electrons in liquid water (1 g/cm^3 density) are shown in Fig. 13.4(a). Each plotted dot represents an interaction event, with the type of interaction being given by its colour. To simplify the plot, tracks have

AQ2

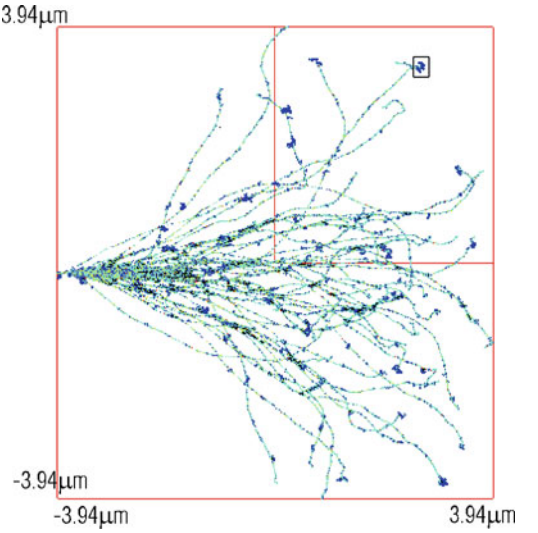

Fig. 13.4 Electron track simulation with the preset LEPTS (Low Energy Particle Track Simulation) code. **(a)** Fully simulated tracks for 50 electrons with energies from 15 keV incident energy to their final thermalisation. **(b)** Nanovolume obtained by "zooming up" the end of one of the tracks as indicated by the small box in (a); the dots' colour indicates the type of interaction event (•, elastic; •, rotational excitation; •, vibrational excitation; •, neutral dissociation; •, ionization)

Table 13.1 Results on the energy deposition and interaction processes derived from the simulation of 50 electron tracks in liquid water for 15 keV incident energy

	Whole irradiated area	End track nanovolume
Volume	4.72×10^{-7} mm^3 (472 μm^3)	5.63×10^{-17} mm^3 (56.3 nm^3)
Total number of interactions:	1490019	273
– Elastic	1083817	214
– Rotational excitation	310899	40
– Vibrational excitation	55692	9
– Electronic excitation	2125	–
– Neutral dissociation	11773	3
– Ionisation	25201	7
– Auger electron generation	197	–
– Electron attachment	309	–
Energy deposition (inelastic)	738.3 keV (1.18×10^{-13} J)	190.4 eV (3.06×10^{-17} J)
Absorbed dose	$2.5 \cdot 10^5$ Gy	$5.4 \cdot 10^{11}$ Gy

been projected onto the YZ plane. Fig. 13.4(b) shows a magnified region of a three-dimensional nano-volume around the end of one of the tracks. Representative information provided by the LEPTS model, for both target volumes, is summarised in Table 13.1. As can be seen in this table, modelling at the molecular level provides not only information about energy deposition but also a detailed description of the type of interaction taking place in the target volume. By reducing the region of

interest to the nano-scale, it is obvious that absorbed dose is not a good quantity to describe radiation effects (see the absorbed dose values in Table 13.1). However the level of detail given by our LEPTS model allows us to develop new tools for nanodosimetry, based on the number of ionisation events or, even more properly, the number of molecular dissociations induced in the nano-volume. Note that for this example we are only showing the total number of ionisations, but this simulation also gives the number and type of ionic fragments produced which together with the information on neutral dissociation and dissociative electron attachment will allow us to characterise radiation effects in terms of structural molecular alterations.

Acknowledgments Work presented in this contribution has been partially supported by the following projects and institutions: Ministerio de Ciencia e Innovación (Project FIS2009-10245), EU Framework Programme (COST Action MP1002) and the Australian Research Council through its Centres of Excellence program.

References

1. R.R. Wilson Phys. Rev. **86**, 261–269 (1952)
2. J.C. Butcher, H. Messel, Phys Rev **112**, 2096–2106 (1958)
3. J.C. Butcher, H. Messel Electron number distribution in electron-photon showers in air and aluminium absorbers. Nucl Phys **20**, 15–128, (1960)
4. A.A. Varfolomeev, I.A. Svetlolobov, Sov Phys JETP **36**, 1263–1270 (1959)
5. C.D. Zerby, H.S. Moran, *A Monte Carlo calculation of the three-dimensional development of high-energy electron-photon cascade showers*. Report ORNL-TM-422, Oak Ridge Natinoal Laboratory (Oak Ridge, Tennessee, 1962)
6. C.D. Zerby, H.S. Moran, J Appl Phys **34**, 2445–2457 (1963)
7. H.H. Nagel, *Die Berechnung von Elektron-Photon-Kaskaden in Blei mit Hilfe der Monte-Carlo Methode*. Dissertation (Rheinische Friedrich-Wilhelms-Universität, 1964)
8. H.H. Nagel, Z Phys **186**, 319–346 (1965)
9. M.J. Berger, Monte Carlo calculation of the penetration and diffusion of fast charged particles. In: B. Alder, S. Fernbach, M. Rotenberg (ed) *Methods in Computational Physics*, vol 1 (Academic, New York, 1963)
10. I. Kawrakow, M. Fippel, Phys Med Biol **45**, 2163 (2000)
11. I. Kawrakow, E. Mainegra-Hing, D.W.O. Rogers, F. Tessier, B.R.B. Walters, *The EGSnrc Code System: Monte Carlo Simulation of Electron and Photon Transport*. Technical report PIRS-701, National Research Council of Canada (Ottawa, 2000)
12. M.J. Berger, S.M. Seltzer, Phys Rev C **2**, 621–631 (1970)
13. M.J. Berger, S.M. Seltzer, *ETRAN Monte Carlo code system for electron and photon transport through extended media*. RSIC Report CCC-107, Oak Ridge National Laboratory (Oak Ridge, 1973)
14. J. Baró, J. Sempau, J.M. Fernández-Varea, F. Salvat, Nucl Instrum Meth Phys Res B **100**, 31–46 (1995)
15. F. Salvat, J.M. Fernández-Varea, J. Sempau, PENELOPE. *A code system for Monte Carlo simulation of electron and photon transport*. OECD-Nuclear Energy Agency (2003)
16. A. Muñoz, J.M. Pérez, G. García, F. Blanco, Nucl Instrum Meth A **536**, 176–188 (2005)
17. M.C. Fuss, A. Muñoz, J.C. Oller, F. Blanco, M.-J. Hubin-Franskin, D. Almeida, P. Limão-Vieira, G. García, Chem Phys Lett **486**, 110–115 (2010)
18. S. Agostinelli et al., Nucl. Instrum. Meth. Phys. Res. .A, **506**(3), 250–303 (2003)

19. A.F. Bielajew, H. Hirayama, W.R. Nelson, D.W.O. Rogers, *History, overview and recent improvements of EGS4*. Report SLAC-PUB-6499, Stanford Linear Accelerator Centre (1994)
20. I. Kawrakow, Med Phys **27**, 485–498 (2000)
21. J.A. Halbleib, T.A. Melhorn, *ITS: The integrated TIGER series of coupled electron/photon Monte Carlo transport codes*. Report SAND84–0573, Sandia National Laboratory (Albuquerque, 1984)
22. F.B. Brown, *MCNP — A general Monte Carlo-particle transport code, version 5*. Report LA-UR-03, Los Alamos National Laboratory (Los Alamos, 2003)
23. W. Friedland, P. Jacob, P. Kundrát, Radiat. Res. **173**, 677–688 (2010)
24. C. Champion, C. Le Loirec, B. Stosic, *Int. J. Radiat. Biol*., submitted
25. Muñoz A, Blanco F, Oller JC, Pérez JM, García G (2007) Adv Quant Chem **52**, 21–57
26. J. Allison et al., IEEE Transactions on Nucl. Sci. **53**(1), 270–278 (2006)
27. J. Apostolakis et al., Radiat. Phys. Chem. **78**(10), 859–873 (2009)
28. S. Incerti, H, Seznec, M. Simon, P. Barberet, C. Habchi, P. Moretto, Radiat. Prot. Dosim. **133**(1), 2–11 (2009)
29. A. Le Postollec, S. Incerti, M. Dobrijévic, L. Desorgher, G. Santin, P. Moretto, O. Vandenabeele-Trambouze, G. Coussot, L. Dartnell, P. Nieminen, Astrobiol. **9**(3), 311–323 (2009)
30. S. Incerti, G. Baldacchino, M. Bernal, R. Capra, C. Champion, Z. Francis, P. Guèye, A. Mantero, B. Mascialino, P. Moretto, P. Nieminen, C. Villagrasa, C. Zacharatou, Int. J. Model. Simul. Sci. Comput. **01**(02), 157 (2010)
31. Z. Francis, S. Incerti, R. Capra, B. Mascialino, G. Montarou, V. Stepan, C. Villagrasa, Appl. Radiat. Isot. **69**(1), 220–226 (2011)
32. S. Incerti, A. Ivanchenko, M. Karamitros, A. Mantero, P. Moretto, H.N. Tran, B. Mascialino, C. Champion, V.N. Ivanchenko, M.A. Bernal, Z. Francis, C. Villagrasa, G. Baldacchino, P. Guèye, R. Capra, P. Nieminen, C. Zacharatou, Med. Phys. **37**(9), 4692 (2010)
33. Z. Francis, C. Villagrasa, I. Clairand, Comput. Meth. Progr. Biomed. **101**(3), 265–270 (2011)
34. H. Nikjoo, S. Uehara, D. Emfietzoglou, F.A. Cucinotta, Radiat. Measurem. **41**(9–10), 1052–1074 (2006)
35. J. Sempau, E. Acosta, J. Baró, J.M. Fernández-Varea, F. Salvat, Nucl Instrum Meth Phys Res B **132**, 377–390 (1997)
36. F. Salvat, J.M. Fernández-Varea, J. Sempau, *PENELOPE-2008: A Code System for Monte Carlo Simulation of Electron and Photon Transport* (Issy-les-Moulineaux, France: OECD/NEA Data Bank 2009). http://www.oecd-nea.org/science/pubs/2009/nea6416-penelope.pdf
37. J. Sempau, J.M. Fernández-Varea, E. Acosta, F. Salvat, Nucl. Instrum. Meth. B **207**, 107–123 (2003)
38. F. Salvat, J.M. Fernández-Varea, Metrologia **46**, S112–S138 (2009)
39. F. Salvat, A. Jablonski, C.J. Powell, Comput. Phys. Commun. **165**, 157–190 (2005)
40. ICRU Report 77, *Elastic Scattering of Electrons and Positrons* (ICRU, Bethesda, MD, 2007)
41. D. Liljequist, J. Phys. D: Appl. Phys. **16**, 1567–1582 (1983)
42. R.M. Sternheimer, Phys. Rev. **88**, 851–859 (1952)
43. ICRU Report 37, *Stopping Powers for Electrons and Positrons*, (ICRU, Bethesda, MD, 1984)
44. D. Bote, F. Salvat, Phys. Rev. A **77**, 042701 (2008)
45. S.M. Seltzer, M.J. Berger, Nucl. Instrum. Meth. B **12**, 95–134 (1985)
46. S.M. Seltzer, M.J. Berger, At. Data Nucl. Data Tables **35**, 345–418 (1986)
47. E. Acosta, X. Llovet, F. Salvat, Appl. Phys. Lett. **80**, 3228–230 (2002)
48. L. Kissel, C.A. Quarles, R.H. Pratt, At. Data Nucl. Data Tables **28**, 381–460 (1983)
49. D.E. Cullen, J.H. Hubbell, L. Kissel, *EPDL97 The evaluated data library, '97 version*, Report UCRL-50400 vol. 6, rev. 5 (Lawrence Livermore National Laboratory, Livermore, 1997)
50. Brusa D., G. Stutz, J.A. Riveros, J.M. Fernández-Varea, F. Salvat, Nucl. Instrum. Meth. A **379**, 167–175 (1996)
51. F. Sauter, Ann. Phys. **11**, 454–488 (1931)

52. M.J. Berger, J.H. Hubbell, *XCOM: Photon Cross Sections on a Personal Computer*, Report NBSIR 87-3597 (National Bureau of Standards, Gaithersburg, MD, 1987)
53. S.T. Perkins, D.E. Cullen, M.H. Chen, J.H. Hubbell, J. Rathkopf, J. Scofield, *Tables and graphs of atomic subshell and relaxation data derived from the LLNL evaluated atomic data library (EADL), $Z = 1$–100*, Report UCRL-50400 vol. 30 (Lawrence Livermore National Laboratory, Livermore, CA, 1991)
54. J.M. Fernández-Varea, R. Mayol, J. Baró, F. Salvat, Nucl. Instrum. Meth. B **73**, 447–473 (1993)
55. A.J. Walker, ACM Trans. Math. Software **3**, 253–256 (1977)
56. C. Champion, D. Oubaziz, H. Aouchiche, Y.V. Popov, C. Dal Cappello, Phys. Rev. A **81**, 032704 (2010)
57. R. Moccia, J. Chem. Phys., **40**, 2186–2192 (1964)
58. J. Neuefeind, C.J. Benmore, B. Tomberli, P.A. Egelstaff, J. Phys.: Cond. Matter **14**, L429–L433 (2002)
59. H. Aouchiche, C. Champion, D. Oubaziz, Radiat. Phys. Chem. **77**, 107–114 (2008)
60. F. Salvat, Phys. Rev. A, **68**, 012708 (2003)
61. D.R. Bates, H.S.W. Massey, Philos. Trans. R. Soc. London Ser. A **239**, 269–304 (1943)
62. N.T. Padial, D.W. Norcross, Phys. Rev. A **29**, 1742–1748 (1984)
63. A. Jain, Phys. Rev. A **41**, 2437–2444 (1990)
64. M.E. Riley, D.G. Truhlar, J. Chem. Phys. **63**, 2182–2191 (1975)
65. C. Champion, J. Hanssen, P.-A.Hervieux, J. Chem. Phys. **117**, 197–204 (2002)
66. C. Champion, Phys. Med. Biol. **48**, 2147–2168 (2003)
67. C. Champion, Phys. Med. Biol. **55**, 11–32 (2010)
68. R.A. Kendall, T.H.Jr. Dunning, R.J. Harrisson, J. Chem. Phys. **96**, 6796 (1992)
69. C. Møller, M. Plesset, Phys. Rev. A **46**, 618 (1934)
70. J. Tomasi, B. Mennucci, R. Cammi, Chem. Rev. **105**, 2999 (2005)
71. J.J. Olivero R.W. Stagat, A.E.S. Green, J.Geophys. Res. **77**, 4797–4811 (1972)
72. A.E.S. Green, S.K. Dutta, J.Geophys. Res. **72**, 3933 (1967)
73. R.N. Compton, L.G. Christophorou, Phys. Rev. **154**, 110–116 (1967)
74. C. Champion, C. Le Loirec, Phys. Med. Biol. **51**, 1707–1723 (2006)
75. P.-A. Hervieux, O.A. Fojon, C. Champion, R.D. Rivarola, J. Hanssen, J. Phys. B: At. Mol. Opt. Phys. **39**, 409–419 (2006)
76. F. Manero, F. Blanco, G. García, Phys. Rev. A **66**, 032714 (2002)
77. M. Inokuti, Rev. Mod. Phys. **43**, 297 (1971)
78. N.F. Mott, H.S.W. Massey, *The Theory of Atomic Collisions*, 3rd edn. Oxford University Press (1965)
79. A. Muñoz, F. Blanco, G. García, P.A. Thorn, M.J. Brunger, J.P. Sullivan, S.J. Buckman, Int. J. Mass Spectrom. **277**, 175 (2008)
80. M.C. Fuss, A. Muñoz, J.C. Oller, F. Blanco, D. Almeida, P. Limão-Vieira, T.P.D. Do, M.J. Brunger, G. García, Phys. Rev. A **80**, 052709 (2009)
81. J.P. Sullivan, A. Jones, P. Caradonna, C. Makochekanwa, S.J. Buckman, Rev. Scient. Instrum. **79**, 113105 (2008)
82. F. Blanco, G. García, Phys. Lett. A **295**, 178 (2002); Phys. Rev. A **67**, 022701 (2003)
83. J.B. Maljković, A. Milosavljević, F. Blanco, D. Šević, G. García, B.P. Marinković, Phys. Rev. A **79**, 052706 (2009)
84. F. Blanco, G. García, J. Phys. B **42**, 145203 (2009)
85. D.D. Reid, J.M. Wadehra, Phys. Rev. A **50**, 4859 (1994); J.Phys. B **29**, L127 (1996)

AUTHOR QUERIES

AQ1. First author considered as a corresponding author. Please check.
AQ2. Please check the part labels in caption are appropriate.